UHASSELT
KNOWLEDGE IN ACTION

Maastricht University

Faculty of Medicine and Life Sciences
School for Life Sciences
Master of Biomedical Sciences

Master's thesis

From injury to repair: Unraveling the oxidative DNA damage response in NSC-34 motorneurons after traumatic injury

Anouar Dlalat

Thesis presented in fulfillment of the requirements for the degree of Master of Biomedical Sciences, specialization Molecular Mechanisms in Health and Disease

SUPERVISOR :

Prof. dr. David WILSON

MENTOR :

Mevrouw Elle SCHEIJEN

2023
2024

Transnational University Limburg is a unique collaboration of two universities in two countries: the University of Hasselt and Maastricht University.

UHASSELT
KNOWLEDGE IN ACTION

www.uhasselt.be
Universiteit Hasselt
Campus Hasselt:
Martelarenlaan 42 | 3500 Hasselt
Campus Diepenbeek:
Agoralaan Gebouw D | 3590 Diepenbeek

UHASSELT
KNOWLEDGE IN ACTION

Maastricht University

Faculty of Medicine and Life Sciences
School for Life Sciences
Master of Biomedical Sciences

Master's thesis

From injury to repair: Unraveling the oxidative DNA damage response in NSC-34 motorneurons after traumatic injury

Anouar Dlalat

Thesis presented in fulfillment of the requirements for the degree of Master of Biomedical Sciences, specialization Molecular Mechanisms in Health and Disease

SUPERVISOR :

Prof. dr. David WILSON

MENTOR :

Mevrouw Elle SCHEIJEN

UHASSELT

From injury to repair: Unraveling the oxidative DNA damage response in NSC-34 motor neurons after traumatic injury

Anouar Dlalat[1], Elle E.M. Scheijen[1], David Wilson[1]

[1] Neurosciences, Biomedical Research Institute, Universiteit Hasselt,
Agoralaan Gebouw C - B-3590 Diepenbeek, Belgium

*Running title: oxidative DNA damage response in NSC-34 motor neurons after traumatic injury

To whom correspondence should be addressed: David Wilson, Tel:011/269205 (Email: david.wilson@uhasselt.be)

Keywords: Deoxyribonucleic Acid (DNA), Neuroblastoma x Spinal Cord-34 (NSC-34), Spinal Cord Injury (SCI), gamma H2A histone family member (γ-H2AX), P53 Binding Protein 1 (53BP1)

ABSTRACT

Every year, around 500,000 people worldwide suffer life-altering spinal cord injuries (SCI), often due to car crashes or falls. SCI disrupts the vital communication pathways between the brain and the body, leading to paralysis, loss of sensory perception, and disrupted autonomic functions below the injury site (1-3). At the moment, there is no cure for SCI, and current treatments focus on alleviating symptoms through surgery, medication, physical therapy, and assistive devices (4). The pathophysiology of SCI involves two distinct phases: the primary event, which is the immediate result of the injury causing neural tissue destruction, and the secondary phase, which unfolds over hours to days post-injury. The secondary phase is characterized by apoptosis, inflammation, and increased production of reactive oxygen species (ROS) due to mitochondrial dysfunction (4). These elevated ROS levels result in oxidation of DNA. This oxidative DNA damage can lead to DNA strand breaks and mutations, contributing to cell death (5). Current research has primarily concentrated on the period extending from 1 day post-injury (dpi) to 28 dpi. Addressing this gap, this study focused on DNA damage and repair from 1 to 8 hpi in Neuroblastoma x Spinal Cord (NSC-34) motor neurons. Our findings show an increase in APE1 levels between 1 and 4hpi. Furthermore, the temporal profiles of γ-H2AX and 53BP1, reveal a dynamic interplay between DNA damage detection and repair initiation. In conclusion, this study highlights the potential of DNA repair pathways, such as base excision repair (BER) and non-homologous end-joining (NHEJ) as therapeutic targets for SCI.

INTRODUCTION

Every year, around 500,000 people worldwide suffer life-altering spinal cord injuries (SCI), often due to accidents like car crashes or falls. SCI disrupts the vital communication pathways between the brain and the body, leading to paralysis, loss of sensory perception, and disrupted autonomic functions below the injury site (1-3). This devastating condition not only impacts the individual's physical well-being but also poses significant challenges to their quality of life. Currently, there is no cure for SCI and treatments mainly focus on surgery, medication, physical therapy, and supportive devices such as braces or traction (4). Therefore, understanding the underlying pathophysiology of SCI is crucial for developing effective treatments and improving the quality of life of people suffering from SCI.

The pathophysiology of SCI can be categorized into two phases: the primary event and a secondary exacerbation of the injury. The primary event is the causative event and is characterized by the destruction of neural tissue, the axonal network, and the meninges.

The secondary phase starts within hours to days after the injury. It is characterized by apoptosis, the production of pro-inflammatory cytokines by astrocytes, macrophages, and microglia, and an increase in reactive oxygen species (ROS) production due to mitochondrial dysfunction (4). Under normal circumstances, increased ROS levels are counteracted by the antioxidant defense system. However, in the case of SCI, limited levels of antioxidants are present in the spinal cord, resulting in elevated oxidative stress. These elevated ROS levels engage with nitrogenous bases and deoxyribose, causing oxidation of DNA. One of the most well-described DNA oxidations caused by ROS is 8-Oxoguanine (8-oxoG). 8-oxoG is a modified version of guanine, which differs from normal guanine because of the addition of an oxygen atom at the eighth position of the guanine molecule. Oxidation of DNA can result in double helix breaks or alterations in DNA bases, potentially leading to mutagenesis or apoptosis (5).

However, the timing and severity of oxidative DNA damage in SCI pathology remains unclear; *Leski et al.* (2001) showed a significant increase in 8-oxodG levels (SCI/Sham rats) at 3 and 6 hours post-injury (hpi) (7). In contrast, *Kotripatruni et al.* (2011) described a significant increase in 8-oxoG levels (SCI/Sham rats) ranging from 1 to 21 days post-injury (dpi) (6). This demonstrates the variety in existing literature about oxidative DNA damage after SCI. Moreover, the cell typing profile of 8-oxoG after SCI remains unknown.

In addition to oxidative base lesions, ROS can also attack the phosphodiester backbone of DNA, resulting in DNA strand breaks. Single Stranded Breaks (SSBs) occur if one DNA strand is broken, whereas double-stranded breaks (DSBs) occur when both strands are broken (6). DNA strand breaks have been measured in literature in various ways, including comet assays and stainings for DNA strand break markers, e.g., phosphorylated Histone H2A variant X (γ-H2AX) and poly(ADP-ribose) (PAR) (7). In response to double-stranded DNA breaks, H2AX gets phosphorylated by kinases such as ataxia telangiectasia mutated (ATM) and ATM-Rad3-related (ATR). This phosphorylation is the initial step in recruiting and localizing DNA repair proteins. (8). In contrast to the DSB-sensing marker γ-H2AX, PAR participates in the signaling of SSBs. PAR polymerase (PARP) is an enzyme that catalyzes the addition of ADP-ribose (ADPR) units to histones and DNA repair enzymes in case of DNA damage. This process, called PARylation, has several essential functions in the DNA damage response, including triggering a cascade of events that lead to the activation of DNA repair pathways, protecting DNA from further damage by providing an energy source for repair enzymes, and directly participating in DNA repair by recruiting repair enzymes to the site of damage (8,9). In current literature, there remains unclarity about both the severity and timing of DNA strand breaks in SCI (7). While *Ozgonul et al.* (2012) described a significant increase in DNA strand breaks in SCI rats compared to the Sham group at 7 and 28 days post-injury (dpi) (10) and *Paterniti et al.* (2010) showed increased PAR staining levels in SCI mice compared to Sham mice (11). However, there still remains a critical gap in the literature about DNA-strand breaks between 1 hpi and 1 dpi because current literature merely studied DNA-strand breaks from 1 dpi to 28 dpi (7).

The types of DNA damage discussed in the preceding paragraphs, i.e., oxidative DNA damage and DNA strand breaks, can trigger critical consequences such as mutagenesis, apoptosis, or senescence. To prevent these processes, neurons possess several DNA repair mechanisms to repair the damaged DNA (12). Base Excision Repair (BER) is the main pathway for repairing oxidative DNA damage. BER occurs by two general pathways: a short-patch and a long-patch repair. A single nucleotide is removed and replaced in short-patch repair, while two nucleotides or more are replaced in long-patch repair. Both short- and long-patch repair function according to the following mechanism: Firstly, BER is initiated by the enzyme DNA glycosylase, which recognizes and excises the damaged bases. Subsequently, the enzyme Apurinic/apyrimidinic endonuclease 1 (APE1) cleaves the DNA backbone, resulting in a nick. Finally, one or more nucleotides will be inserted at the nicked site and sealed by DNA ligase (12). DSBs, on the other hand, are mainly repaired by Non-Homologous End-Joining (NHEJ) and Homologous recombination (HR) (13). NHEJ is a fast and error-prone method that simply rejoins the broken DNA ends. While

efficient, it can occasionally introduce mutations. NHEJ involves recognizing the damage, trimming the broken ends, and finally ligating them together (13). HR, in contrast, is an accurate mechanism utilizing an intact, identical DNA strand as a template to repair the damaged one. However, due to its reliance on an identical template, HR is primarily active during the synthesis (S-phase) and Gap 2 (G2-phase) of the cell cycle, where such a template is readily available (13). Although neuronal cells possess HR machinery, its activity in mature neurons is limited due to their post-mitotic character. The role of DNA repair in SCI remains a subject of ongoing discussion. *Kotipatruni et al.* (2011) found a significant increase in mRNA levels and protein levels of various BER enzymes in SCI rats versus Sham rats, including DNA glycosylase and APE1 (16). In contrast, other studies found decreased mRNA and protein levels of BER-related enzymes in SCI (14,15).

Based on the existing gaps in current literature regarding DNA damage and repair in SCI, this study aims to investigate the oxidative DNA damage response in NSC-34 motor neurons after traumatic injury. NSC-34 is a hybrid cell line generated by fusing mouse motor neuron precursors with neuroblastoma cells (16). Utilizing a differentiated NSC-34 motor neuron model provides a controlled and reproducible system for studying neuronal DNA damage and repair.

EXPERIMENTAL PROCEDURES

Cell culture

The NSC-34 cell line, a Mus musculus neuroblastoma-spinal cord hybrid cell line, was cultured using Dulbecco's Modified Eagle Medium (DMEM, 41966-029 Gibco) supplemented with 10% heat-inactivated fetal bovine serum (FBS), and 1% Penicillin/Streptomycin. Cultures were maintained at 37°C and 5% CO2 in a humidified incubator. Cells were seeded at 5000 cells/cm^2 in Nunc Delta Surface 96-well plates coated with 2% gelatin. After 24 hours, the cells were differentiated for 96 hours by differentiation medium containing DMEM/F-12, 1% FCS, 1% NEAA, 0.5% Penicillin/Streptomycin, and 1 µM all-trans retinoic acid (atRA).

Scratch assay

After 96 hours of differentiation, an 800 micrometre scratch was induced by utilizing the Sartorius Essen 96 wound maker.

qPCR

RNA was extracted to validate the differentiation of NSC-34 cells to motor neurons. Firstly, the samples were lysated using Qiazol (Qiagen, 79306). For RNA extraction, chloroform was added to the samples and the solution was centrifuged at 14 000 rpm for 15 minutes at 4°C. Next, the solutions were incubated with 2-isopropanol for 30 minutes at room temperature and centrifuged for 10 minutes at 4°C and 14000 rpm. The obtained RNA pellets were washed twice with 75% cold (4°C) ethanol and centrifuged for 10 minutes at 4°C and 14000 rpm. Following air drying, the RNA pellets were resuspended in milliQ (MQ), and the purity of the RNA was assessed using the NanoDrop® ND-1000 spectrophotometer (ThermoFisher). Next, cDNA synthesis was conducted using PrimeScript RT reagent kit (Takara Bio, RR037A). For qPCR, a StepOnePlus Real-Time PCR System was used along with a master mix consisting of the specified primer pairs (Supplementary table 1), TB Green, ROX and MilliQ. The qPCR was performed with the following parameters: 95°C for 30 seconds (initial denaturation), 95°C for 5 seconds, and 60°C for 30 seconds (PCR stage) for 40 times, then 95°C for 15 seconds, 60°C for 1 minute, and 95°C for 15 seconds (dissocation stage). To calculate fold changes, the ΔΔCt method was employed.

Immunocytochemistry

NSC-34 motor neurons were fixated with 4% paraformaldehyde for 30 min. Then, the cells were washed with Tris Buffered Saline (TBS) and permeabilized with 2% Triton in TBS for 10 min at room temperature. Subsequently, a blocking solution composed of 10% goat serum

in TBD (TBS + 0.1% Triton-X100) was added for 1 hour. An immunocytochemical analysis was performed on scratched and unscratched NSC-34 derived motor neurons for the DNA damage markers γ-H2AX (rabbit, 1/400, Bioké, 2577), 53BP1 (rabbit, 1/1000, Novus Biologicals, NB100-304), PAR (rabbit, 1/500, Abcam, ALX-804-220-R100) and DNA repair marker APE1 (rabbit, 1/100, Novus Bio, NB100-101). The primary antibody diluted in blocking solution was added and incubated overnight at 4°C. Following overnight incubation, the cells were washed three times with TBD and the secondary antibody (Supplementary table 2) diluted in blocking buffer (1:800) was added and incubated for 1h. Finally, the cells were washed with TBD 3 times and DAPI (1/10000) was added for 10 min at room temperature, after which the cells were washed with TBS twice for 5 minutes and left on TBS until imaging by using the Nikon Eclipse Ti2-E fluorescence microscope.

Image analysis

Quantitative analysis of the images was conducted using ImageJ with a selfmade script (Supplementary table 3). Images were loaded, and the channels were split and subjected to a Gaussian Blur with a 5.00 radius. Background subtraction was applied to all channels using a rolling ball radius of 50. Thresholding adjustments, standardized across experiments, were performed manually once for each staining using Otsu's model. Cells were separated using watershed segmentation, and particle analysis was conducted on both channels. This analysis facilitated the calculation of the percentages of negative, foci, and positive cells, as well as the average foci count per cell. This was performed by utilizing the 'Find maxima' function to identify potential foci within the nuclei. To accurately count the foci, the noise tolerance parameter was adjusted. This step was critical to differentiate true foci from background noise.
The 'Preview Point Selection' option was used to visually examine the effectiveness of the noise tolerance settings.

Neuronal outgrowth method

The neurite length assay was performed using ImageJ software. For each image, the length of 30 randomly selected neurites was measured from the edge of the cell body to the tip of the neurite. Measurements were taken by drawing a straight line along the length of each neurite using the built-in measurement tool in ImageJ. This process was manually performed to ensure accurate alignment with the neurite's trajectory.

Statistics

Statistical analyses were conducted using GraphPad Prism software 10.1.2. The homoscedasticity and normality of the data were assessed using the Brown-Forsythe and Shapiro-Wilk Test. In case of normally distributed and homoscedastic data, an unpaired t-test was performed in case of 2 independent groups and a One-Way ANOVA if there were groups or more followed by a Tukey HSD. If the data did not meet the assumptions of normality and homoscedasticity, a Mann-Whitney test was employed in case of 2 independent groups and a Kruskall Wallis test if there were 3 groups or more, followed by a Dunn's test. P-Values smaller or equal to 0,05 were considered statistically significant.

RESULTS

Successful differentiation of NSC-34 cells to NSC-34 motor neurons

Firstly, we aimed to validate the differentiation of NSC-34 cells into motor neurons to ensure that our observations on DNA damage and repair mechanisms would be conducted on cells that mimic motor neuron physiology. In Figure 1, the differentiation process was successfully confirmed through a multi-faceted approach, incorporating morphological, quantitative, and molecular assessments. Microscopic images (Fig 1a) at 20x magnification provided the initial evidence of differentiation, showing a clear morphological distinction between undifferentiated NSC-34 cells and differentiated NSC-34 derived motor neurons. The differentiated cells, which had been cultured in differentiation medium for 96 hours, displayed a higher neurite length relative to the cell body. This morphological change was quantitatively supported by a neurite length assay (Fig 1B), which showed a statistically significant increase in neurite length over the cell body for the differentiated cells, confirming the visual observations of Fig 1A. To further substantiate the differentiation at the molecular level, qPCR analyses were performed to measure the expression of several neuronal markers. Notably, VACHT, involved in the synthesis of the neurotransmitter acetylcholine; ACHE, an enzyme that breaks down acetylcholine; RBFOX3, a neuronal nucleus marker; MAP2, a marker for dendritic structure and stability; MAPT, also known as Tau, associated with microtubule assembly; GAP43, indicative of axonal growth and synaptic plasticity, and CHAT, choline acetyltransferase, essential for synthesizing acetylcholine, were all significantly upregulated in the differentiated cells compared to the undifferentiated controls (Fig 1C), further confirming the successful differentiation of NSC-34 cells into motor neurons.

Challenges in detecting oxidative DNA damage in NSC-34 motor neurons after traumatic injury

Following our confirmation that NSC-34 cells had differentiated into motor neurons, we moved on to study whether these motor neurons exhibit oxidative DNA damage after a traumatic injury. In our exploration of DNA damage within NSC-34-derived motor neurons, we initially attempted to utilize 8-oxoguanine as a marker for oxidative DNA damage; however, this approach proved unsuccessful due to scientific challenges (Supplementary Figure 1). Notably, the 8-oxodG antibody stained the cell body rather than the nuclei, indicating a lack of specificity.

Increasing trend in APE1 levels in NSC-34 motor neurons after traumatic injury

Consequently, our attention turned to APE1, a pivotal marker within the base excision repair (BER) pathway, which is integral to the repair of oxidative DNA lesions (Figure 2). Fig 2A illustrates a progressive increase in APE1 expression from 1 to 4hpi, whereas Fig 2B provides a detailed view of the different conditions, demonstrating the nuclear localization of APE1. Furthermore, a quantitative assessment confirms an increasing trend in APE1 expression from 1 to 4 hpi (Fig 2C), suggesting an increase in BER activity during this period. However, APE1 levels appeared to plateau between 4 and 8 hpi.

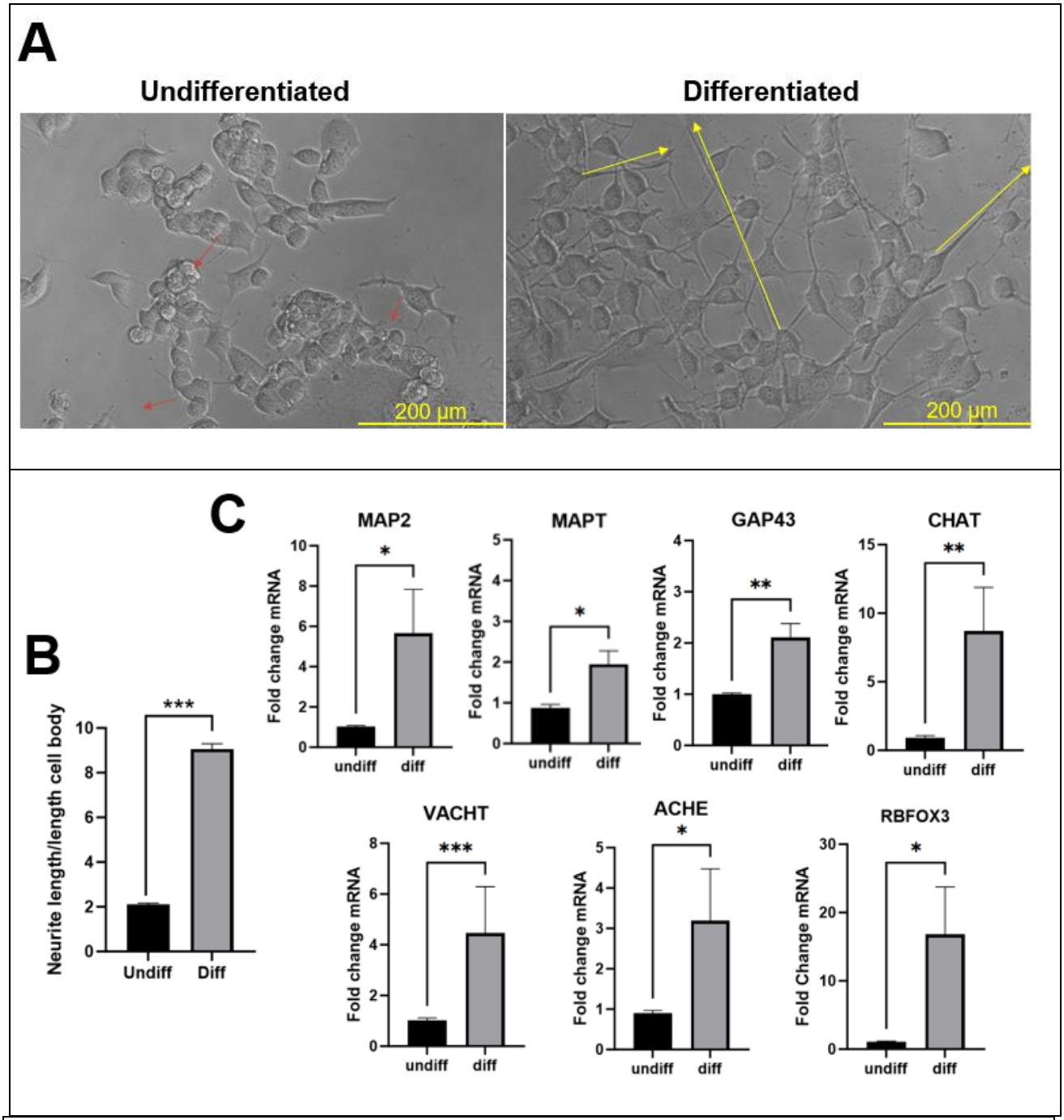

Figure 1: Differentiation of NSC-34 cells to motor neurons increases neurite length and gene expression of neuronal markers (A) Microscopic images taken at 20x magnification of undifferentiated NSC-34 cells (left) showing short neurites (red arrows) and differentiated NSC-34 cells (right) displaying long neurites with many branches and interconnections (yellow arrows). (B) Neurite length assay confirming that the neurite length relative to the cell body is significantly higher in the differentiated NSC-34 cells compared to the undifferentiated cells. N = 3, unpaired t-test, *** $p < 0.0005$. (C) qPCR analyses validating the differentiation of NSC-34 cells into motor neurons. N=4, unpaired t-test. * $p < 0.05$, ** $p < 0.005$, *** $p < 0.0005$.

Difficulties in assessing Single Stranded Breaks (SSBs) in NSC-34 motor neurons after traumatic injury

In the continuation of our study on the oxidative DNA damage response in NSC-34 derived motor neurons post-traumatic injury, we extended our analysis beyond the base excision repair (BER) pathway to examine single-stranded breaks (SSBs). Our initial attempts to utilize PAR as a marker for SSBs were met with scientific challenges (Supplementary Figure 2), similar to those encountered with 8-oxoguanine, leading us to exclude PAR from our set of reliable markers.

Elevated levels of γ-H2AX in NSC-34 motor neurons post traumatic injury

Subsequently, we focused on the most severe type of DNA damage; Double Stranded Breaks (DSBs). The first marker we investigated for DSBs is γ-H2AX (figure 3). In case of a DSB, the H2ax protein gets phosphorylated on the serine residue at position 139, thereby resulting in the phosphorylated version, γ-H2AX. This post-translational modification is a crucial part of the cellular response to DNA damage, marking the sites of DSBs and recruiting DNA repair proteins such as 53BP1 (8). Hence, we examined the ICC profiling of γ-H2AX after traumatic injury and made a distinction between three different cell types (Fig 3A); negative cells (Fig 3A left panel), cells showing foci (Fig 3A middle panel) and pan nuclear cells (Fig 3A right panel). Negative cells showed no detectable levels of γ-H2AX, indicating an absence of marked DNA damage. Cells with foci exhibited discrete foci of γ-H2AX, which are indicative of localized DNA DSBs. Pan nuclear cells displayed widespread γ-H2AX expression throughout the nucleus, suggesting extensive DNA damage and a pre-apoptotic state. ICC images of γ-H2AX expression show an increase in γ-H2AX levels from 1 to 4hpi, followed by a decrease from 4hpi to 8hpi (Fig 3B) In Fig 3B, the top series reveal the full scope of the well, highlighting the scratch lesion. Whereas the bottom series presents a magnified examination. In addition, we notice an increasing trend in the proportion of cells with foci from 1 to 4hpi, followed by a decrease from 4hpi to 8hpi (Fig 3C). Furthermore, we found that the average number of foci per cell was significantly higher at 2hpi and 4hpi compared to the unscratched, 1hpi and 4hpi condition (Fig 3D).

Increased 53BP1 expression in NSC-34 motor neurons after traumatic injury

Expanding on our findings from Figure 3, we investigated 53BP1, another crucial marker for DSBs. 53BP1 is recruited to regions marked by γ-H2AX, where it plays a pivotal role in facilitating repair processes. Specifically, it is involved in the non-homologous end joining (NHEJ) pathway (17,18). In Figure 4, we focused on investigating 53BP1 as a marker for DSBs. Similar to Figure 3, Figure 4A classifies NSC-34 derived motor neurons into three categories based on their 53BP1 expression: negative (Fig 4a left panel), foci (fig 4A middle panel), and pan-nuclear cells (Fig 4A right panel). ICC analysis of 53BP1 showed an increase in 53BP1 expression from 1 to 8hpi (Fig 4B). The top series displays a comprehensive view of the well (Fig 4B upper panel), highlighting the area of the scratch injury. In contrast, the bottom series provides an enlarged perspective of the cells (Fig 4B). Moreover, we noticed a significant increase in the proportion of cells in a foci state at 4hpi and 8hpi compared to the unscratched, 1hpi, and 2hpi conditions (Fig 4C). Notably, the proportion of cells in a foci state at 8 hpi also significantly surpassed that at 4 hpi (Fig 4C). Finally, we observed a significantly higher foci count per cell at 4hpi and 8hpi in comparison with the unscratched, 1hpi, and 2hpi conditions (Fig 4D).

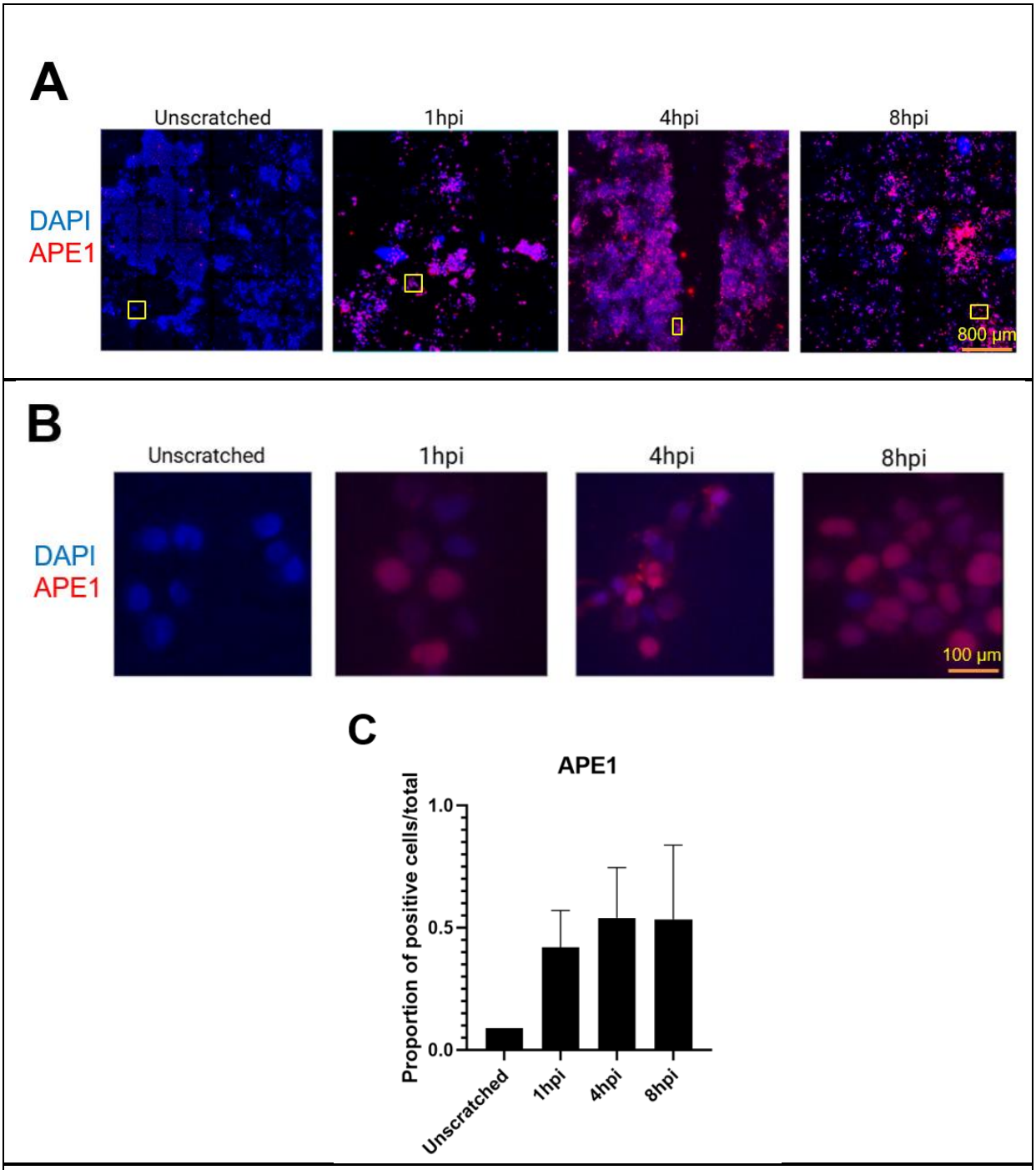

Figure 2: Increasing trend in APE1 levels in NSC-34 motor neurons after traumatic injury. (A) Immunocytochemistry (ICC) analyis images for APE1, a marker for DNA repair, in NSC-34 derived neurons following scratching at 1,4 and 8 hours post-injury (hpi), showing an increase in APE1 levels from 1 to 4hpi. (B) Zoomed images of the different conditions showing that APE1 is specifically expressed within the nuclei. (C) Quantification of the proportion of positive cells for APE1 staining displaying an increasing trend from 1 to 4hpi and a plateau phase between 4hpi and 8hpi.. N = 1-2. One-Way ANOVA, followed by a Tukey HSD. p = 0.4884.

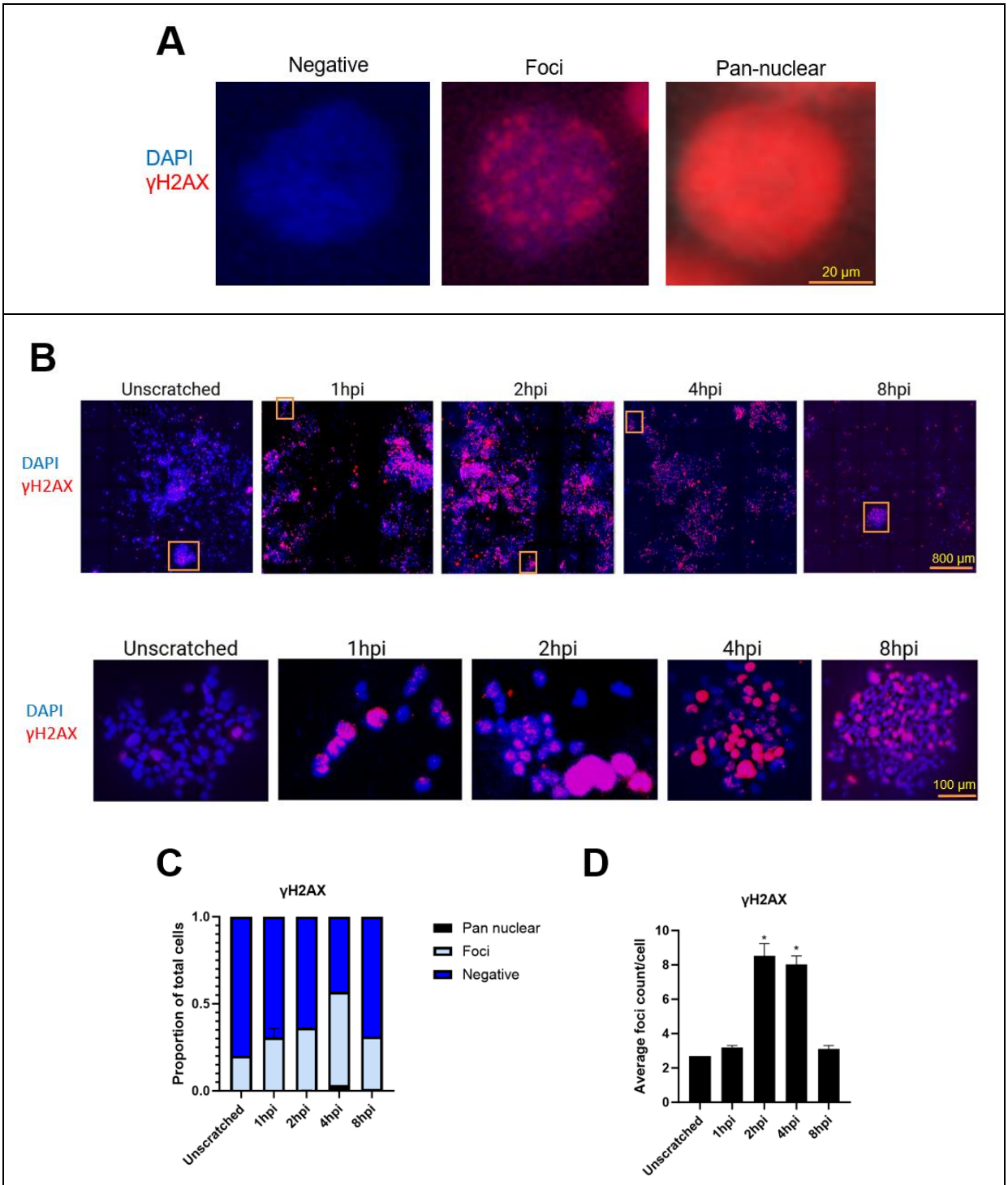

Figure 3: Increased γ-H2AX levels in NSC-34 motor neurons after traumatic injury. (A) Representative images of three distinct cell types: negative (left), foci (middle), and pan nuclear (right). (B) ICC images for γ-H2AX showing an increase in γ-H2AX levels from 1hpi to 4hpi and a decrease from 4hpi to 8hpi. The upper row shows the entire well, including the scratch site, while the lower row provides zoomed-in views of the various conditions. (C) Quantification of the proportion of negative, foci, and pan nuclear cells displaying an increasing trend in the proportion of cells with foci from 1 to 4hpi, followed by a decrease from 4hpi to 8hpi. N = 1-2. One-Way ANOVA, Tukey HSD. P = 0,1219. (D) The average foci count per cell was significantly elevated at 2 and 4 hpi, compared to the unscratched, 1hpi and 8hpi conditions. N =1-2. One-way ANOVA, Tukey HSD. *p < 0.05.

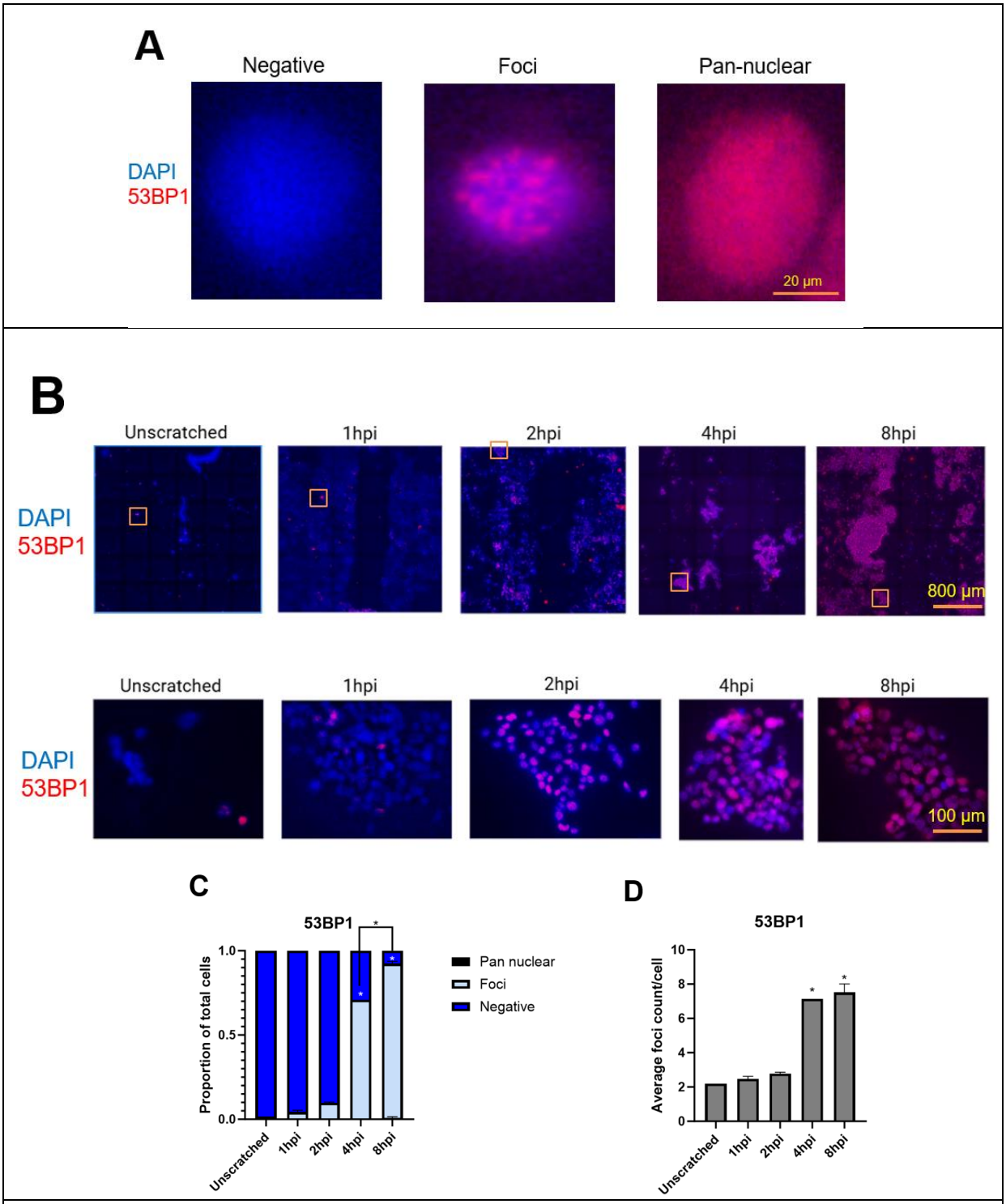

Figure 4: Elevated 53BP1 levels Post-Scratch Injury in NSC-34 Derived Motor neurons. (A) Representative images showing cell classification: negative (left), foci (middle) and pan nuclear (right) (B) ICC images display an increase in 53BP1 expression from 1 to 8hpi. The upper panel shows the entire well and the lower panel provides a zoomed-in view. (C) Quantification of negative, foci and pan nuclear cells showing an increase in the proportion of cells with foci at 4 and 8hpi, compared to the unscratched, 1hpi and 2hpi condition. Notably, the proportion of foci-bearing cells at 8hpi also significantly surpassed that at 4hpi. N =1-2. One-way ANOVA and Tukey HSD. * $p < 0.05$ (D) The foci count per cell at 4 and 8hpi was significantly higher than the unscratched, 1hpi, and 2hpi conditions. N=1-2. One-way ANOVA and Tukey HSD. * $p < 0.05$

DISCUSSION

This study utilized the NSC-34 cell line, a well-established *in vitro* model derived from mouse motor neuron precursors fused with neuroblastoma cells, to investigate the oxidative DNA damage response following traumatic injury (16). We utilized retinoic-acid to induce differentiation from NSC-34 cells to motor neurons, as well as several other studies in literature (19-21). Whereas other studies utilized Prostaglandin E2 as a compound to induce differentiation from NSC-34 cells to motor neurons (22,23). Prostaglandin E2 is favoured for its rapid induction of morphological differentiation, which is beneficial when time is a critical factor (22). Retinoic acid, on the other hand, typically requires a longer period to achieve similar levels of neuritogenesis, but is the most extensively documented differentiating agent in literature (16,21).

Successful validation of differentiation of NSC-34 cells to motor neurons

The differentiation of NSC-34 cells into motor neurons was successfully validated through morphological, quantitative, and molecular assessments (Figure 1). This differentiation was critical to ensure that our observations on DNA damage and repair were conducted on cells mimicking motor neurons *in vitro*. Several studies also confirmed the differentiation of NSC-34 to motor neurons by using a morphological comparison between undifferentiated and differentiated cells (16,24) . For quantification of these morphological differences, we compared the neurite length over the cell body, whereas other studies have been looking at the neurite length per cell (16,20). Our method considers variations in neuron size by emphasizing the proportion of neurite length relative to the cell body. Furthermore, various other studies successfully confirmed the differentiation by performing qPCR analyses (16,24). Another method that could be interesting to validate the differentiation is Whole-cell Patch Clamp (22). The Whole-cell Patch-Clamp technique is a powerful method in electrophysiology used to study ionic currents in individual living cells (25). Demonstrating a lower current threshold for action potentials through this method can be indicative of a more efficient neuronal differentiation process (22).

Inducing traumatic injury by a scratch assay

Following the differentiation of NSC-34 cells into motor neurons, an 800-micrometer scratch was introduced in each well of a 96 well plate using the Sartorius Essen 96 wound maker to simulate injury. Simulating SCI *in vitro* presents significant challenges due to the complexity of the spinal cord's structure and function (26). However, this *in vitro* scratch assay, while a simplified model, offers a reproducible method to investigate DNA damage and repair after injury. Cell lines like NSC-34 provide a uniform and consistent platform for a scratch assay, with advantages including ease of use and rapid proliferation (27). However, they may lack the full physiological relevance compared to primary cells, which better mimic the *in vivo* state but are limited by their finite lifespan and variability between donors (28). In addition, stem cells offer the potential for more physiologically relevant models due to their ability to differentiate into various cell types, yet they pose challenges in terms of complexity and the need for precise control over differentiation processes (29). Considering the practical considerations at the research institute and the issues with contamination, utilizing the NSC-34 cell line was the most feasible approach for studying the oxidative DNA damage response after traumatic injury.

Early Timepoints and increase in BER activity

In our study, we focused on the initial phase post-injury, specifically from 1 to 8 hpi. The rationale behind focusing on the initial 1 to 8hpi in our study was to explore a relatively under-investigated timeframe in SCI research. While most studies examine DNA damage and repair from 1 day post-injury up to 28 days post-injury (dpi), our research aimed to provide insights into the oxidative DNA damage response that occurs shortly after SCI. This early period is critical for understanding the onset of secondary injury mechanisms (7).

Our findings showed an increasing trend in APE1 expression from 1 to 4hpi, a key enzyme in the base excision repair (BER) pathway, suggesting an increase in BER activity between 1 and 4 hpi (Figure 2). This increase likely represents an early cellular response to oxidative DNA lesions,

aiming to mitigate the damage and preserve genomic integrity. However, the expression levels of APE1 appeared to plateau between 4 and 8 hpi, potentially indicating a stabilization of the initial repair response. This plateau could reflect a resolution of oxidative DNA damage or a transition to other repair mechanisms or cellular processes. A study by *Leak et al.* (2015) showed that an increase in APE1 levels can protect hippocampal neurons from ischemic injury by reducing oxidative DNA damage in Traumatic Brain Injury (TBI). This supports the notion that an increase in APE1 levels is an early cellular response to oxidative DNA damage, consistent with our findings.

Temporal pattern of γ-H2AX post-injury shows effective sensing of DSBs

After investigating APE1 levels after traumatic injury, we continued looking at the most severe type of DNA damage: double-strand breaks (DSBs). Firstly, we examined γ-H2AX, which is a critical marker for sensing DSBs (8,17). The increasing trend in the proportion of cells with γ-H2AX foci from 1 hpi to 4 hpi and the elevated number of foci per cell at 2 and 4hpi indicate an accumulation of DSBs between 1 and 4hpi. (Figure 3). There are several possible reasons for this early increase in γ-H2AX. Traumatic injury most likely results in a physical disruption of the DNA, causing a peak in DSBs (30,31). This requires the cell to respond quickly in order to identify and start repair processes, as shown by how quickly γ-H2AX foci form (32). In contrast, there is a decreasing trend in γ-H2AX expression between 4 and 8hpi (Figure 3). A possible explanation for this decrease the fact that NHEJ has successfully resolved a part of the DSBs, thereby reducing the need for γ-H2AX signalling and resulting in dephosphorylation of γ-H2AX (17).

Temporal dynamics of 53BP1 appears complementary to γ-H2AX

Following investigation of γ-H2AX, we examined the temporal pattern of 53BP1 post-injury. 53BP1 is drawn to sites of DNA damage and is essential for the repair of double-strand breaks (17). 53BP1 has been demonstrated to affect the non-homologous end joining (NHEJ) pathway selection for DNA repair (17). The connection between 53BP1 and γ-H2AX is crucial for DNA repair at sites of DSBs (18). 53BP1 uses its BRCT domains, which are phospho-specific interaction motifs, to recognize and bind to γ-H2AX. This binding facilitates the recruitment of other repair factors and thereby promotes the repair of DSBs by stabilizing the accumulation of 53BP1 at the damage sites (18).
Interestingly, the temporal pattern of γ-H2AX and 53BP1 showed complementary dynamics. The early peak in γ-H2AX expression, from 1 to 4 hpi, indicates the initial sensing and signalling phase of the DNA damage response (33). This early phase is crucial for the recruitment of 53BP1 to the sites of DSBs (33) . By 4 hpi, the proportion of cells with 53BP1 foci and the average number of 53BP1 foci per cell has significantly been increased (Fig 4C), suggesting an active engagement of the NHEJ repair pathway, which 53BP1 is critically involved in (34). In addition, the increase in the proportion of cells with 53BP1 foci and the average number of foci per cell from 4 to 8 hpi correlates with the decrease in γ-H2AX levels, showing a transition from damage detection to repair completion. This is supported by an ICC staining (supplementary figure 3) showing negligible to no detectable levels of clCasp3 at 4hpi. Because of time, it was not feasible to perform a clCasp3 staining at the various timepoints (1,2,4 and 8hpi) and compare the amount of apoptosis. An overview of the complementary dynamics of 53BP1 and γ-H2AX is visualized in Figure 5. This interaction between 53BP1 and -H2AX has also been studied in literature in several ways, including a dual immunofluorescence protocol and a proximity ligation assay (35,36).

Limitations and future directions

One of the limitations of our study was the inability to investigate oxidative DNA damage using 8-oxoguanine (8-oxoG, supplementary figure 1) due to non-specific staining issues. Because of this, we also tried a different staining protocol including 10min HCl and Tris incubating steps, with similar results (37). The non-specific staining could be due to a variety of factors, such as antibody cross-reactivity or insufficient washing steps. To address this, we could optimize the staining protocol by having 5 washing steps instead of 3. In addition, success in other studies may be attributed to the use of more specific antibodies. Therefore, using the anti 8-oxoguanine antibody (mouse, 1/200, Abcam, 2Q2311) could be considered.

Our attempts to measure single-strand breaks (SSBs) using poly(ADP-ribose) (PAR, supplementary figure 2) were also unsuccessful, due to similar technical challenges. Utilizing a different protocol including a 5 minute methanol: acetone permeabilization did not succeed. Hence, in future research, the staining protocol should be optimized by having 5 washing steps instead of 3. Additionally, using the PAR/pADPr Antibody (mouse, 1/1000, Biotechne, 4335-MC-100) could be taken into consideration.

In addition, this study did not investigate cell death, which is a crucial component of the secondary injury phase in SCI (38). Cell death mechanisms such as apoptosis contribute significantly to the progression of injury and the overall pathophysiology of SCI (38). Therefore, it could be valuable to include cell death assays, e.g. the TUNEL and Annexin V assay and stainings for apoptosis markers such as cleaved Caspase-3 (39,40).

Furthermore, future research should extend the timepoints of analysis from the initial 8hpi to 1dpi. Although our investigation covered the timeframe from 1 to 8 hpi, existing literature predominantly focuses on periods between 1 dpi and 28 dpi (7). It would also be informative to examine whether DNA damage persists, resolves, or progresses over time. For instance, tracking the movement of DNA damage and repair markers from the injury site (e.g., 0-200 micrometres, 200-400 micrometres, etc.) at later timepoints could reveal spatial and temporal patterns of DNA damage and repair propagation.

Finally, incorporating primary motor neurons isolated from the spinal cords of mice could provide a more physiologically relevant model, offering insights that are more applicable to *in vivo* conditions (27). This approach could help validate findings from NSC-34 cells and potentially uncover differences in DNA damage responses between cell lines and primary cells.

The findings of our study emphasize the critical role of DNA repair pathways in the cellular response to oxidative DNA damage following traumatic injury. The early increase in APE1 levels suggests that the BER pathway is rapidly activated to address oxidative DNA damage. Similarly, the dynamic changes observed in γ-H2AX and 53BP1 expression patterns highlight the increase and subsequent repair of double-strand breaks (DSB) repair via non-homologous end joining (NHEJ). Enhancing the efficacy of these repair mechanisms could reduce the extent of DNA damage, thereby preserving neuronal function and improving recovery outcomes. A possible approach could be intraspinally injecting an adeno-associated viral vector, expressing APE1 (BER) or DNA-PKs (NHEJ) under the neuronal promotor Syn, to ensure neuron-specific expression (41-43).

CONCLUSION

In this study, we investigated the oxidative DNA damage response in NSC-34 motor neurons following traumatic injury. Our findings show an early increase in BER activity, as evidenced by the elevated APE1 levels within the first few hours post-injury. Furthermore, the temporal profiles of γ-H2AX and 53BP1, reveal a dynamic interplay between DNA damage detection and repair initiation. In conclusion, this study highlights the potential of DNA repair pathways, such as base excision repair (BER) and non-homologous end-joining (NHEJ) as therapeutic targets for spinal cord injury.

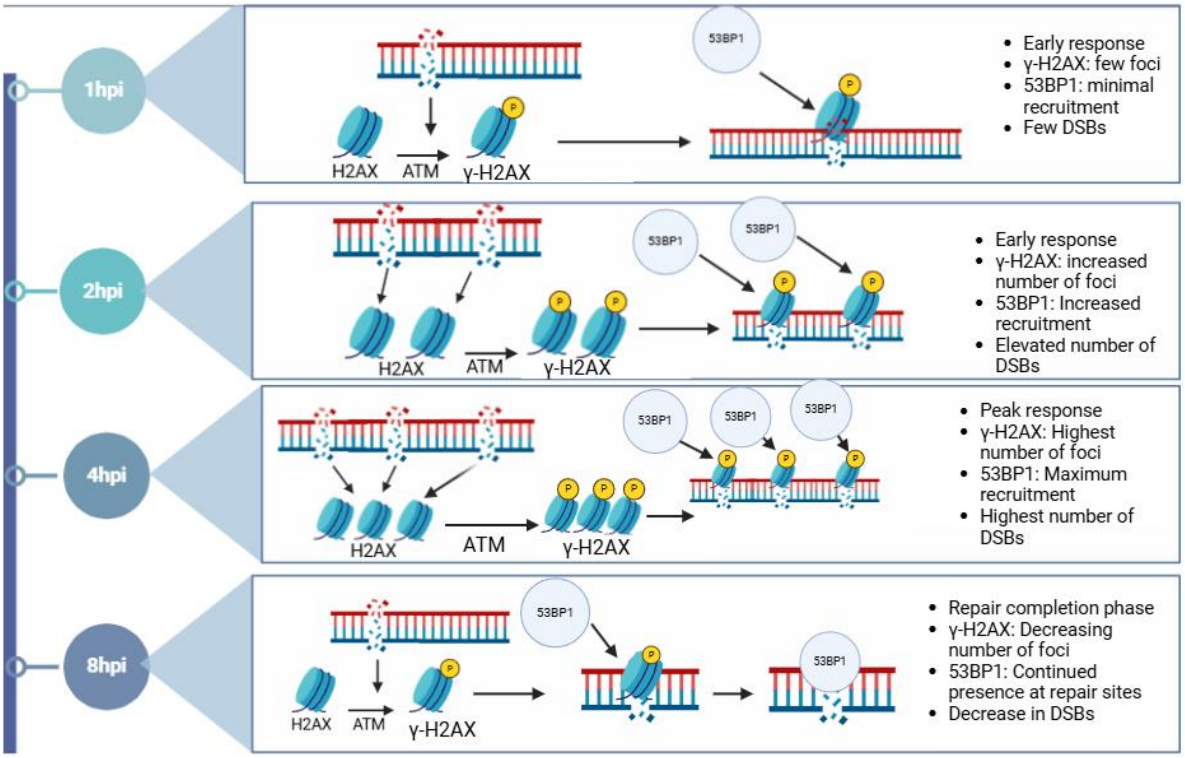

Figure 5: Visualization of the temporal γ-H2AX and 53BP1 levels in NSC-34 motor neurons post-injury. At 1hpi, few DSBs and γ-H2AX foci were present, thereby resulting in a minimal recruitment of 53BP1. At 2hpi, the number of DSBs and γ-H2AX foci increased, leading to an elevated recruitment of 53BP1 and consequent repair of the DSBs. At 4hpi, a peak response was noticed; including the highest number of DSBs and γ-H2AX positive foci, resulting in maximum recruitment of 53BP1 in order to facilitate repair of the DSBs. At 8hpi, there was a repair completion phase. A decrease in the amount of γ-H2AX positive foci was observed, indicating there were less DSBs. However, 53BP1 continued present at the various repair sites. This shows ongoing repair activity, which is consistent with the cellular need to ensure genome stability following extensive DNA damage. ATM: Ataxia-telangiectasia mutated kinase.

REFERENCES

1. Collaborators, G. B. D. N. (2019) Global, regional, and national burden of neurological disorders, 1990-2016: a systematic analysis for the Global Burden of Disease Study 2016. *Lancet Neurol* **18**, 459-480
2. Alizadeh, A., Dyck, S. M., and Karimi-Abdolrezaee, S. (2019) Traumatic Spinal Cord Injury: An Overview of Pathophysiology, Models and Acute Injury Mechanisms. *Front Neurol* **10**, 282
3. Sandean, D. (2020) Management of acute spinal cord injury: A summary of the evidence pertaining to the acute management, operative and non-operative management. *World J Orthop* **11**, 573-583
4. Anjum, A., Yazid, M. D., Fauzi Daud, M., Idris, J., Ng, A. M. H., Selvi Naicker, A., Ismail, O. H. R., Athi Kumar, R. K., and Lokanathan, Y. (2020) Spinal Cord Injury: Pathophysiology, Multimolecular Interactions, and Underlying Recovery Mechanisms. *Int J Mol Sci* **21**
5. Juan, C. A., Perez de la Lastra, J. M., Plou, F. J., and Perez-Lebena, E. (2021) The Chemistry of Reactive Oxygen Species (ROS) Revisited: Outlining Their Role in Biological Macromolecules (DNA, Lipids and Proteins) and Induced Pathologies. *Int J Mol Sci* **22**

6. Kotipatruni, R. R., Dasari, V. R., Veeravalli, K. K., Dinh, D. H., Fassett, D., and Rao, J. S. (2011) p53- and Bax-mediated apoptosis in injured rat spinal cord. *Neurochem Res* **36**, 2063-2074
7. Scheijen, E. E. M., Hendrix, S., and Wilson, D. M., 3rd. (2022) Oxidative DNA Damage in the Pathophysiology of Spinal Cord Injury: Seems Obvious, but Where Is the Evidence? *Antioxidants (Basel)* **11**
8. Kuo, L. J., and Yang, L. X. (2008) Gamma-H2AX - a novel biomarker for DNA double-strand breaks. *In Vivo* **22**, 305-309
9. Wei, H., and Yu, X. (2016) Functions of PARylation in DNA Damage Repair Pathways. *Genomics Proteomics Bioinformatics* **14**, 131-139
10. Ozgonul. (2014) Effects of embryonic neural stem cell therapy on DNA damage products in urine and tissue after spinal cord injury in rats. *Febs Journal*
11. Paterniti, I., Mazzon, E., Emanuela, E., Paola, R. D., Galuppo, M., Bramanti, P., and Cuzzocrea, S. (2010) Modulation of inflammatory response after spinal cord trauma with deferoxamine, an iron chelator. *Free Radic Res* **44**, 694-709
12. Robertson, A. B., Klungland, A., Rognes, T., and Leiros, I. (2009) DNA repair in mammalian cells: Base excision repair: the long and short of it. *Cell Mol Life Sci* **66**, 981-993
13. Mao, Z., Bozzella, M., Seluanov, A., and Gorbunova, V. (2008) DNA repair by nonhomologous end joining and homologous recombination during cell cycle in human cells. *Cell Cycle* **7**, 2902-2906
14. Bao, F., Chen, Y., Dekaban, G. A., and Weaver, L. C. (2004) An anti-CD11d integrin antibody reduces cyclooxygenase-2 expression and protein and DNA oxidation after spinal cord injury in rats. *J Neurochem* **90**, 1194-1204
15. Dagci, T., Armagan, G., Konyalioglu, S., and Yalcin, A. (2009) Alterations in the expression of the apurinic/apyrimidinic endonuclease-1/redox factor-1 (APE/ref-1) and DNA damage in the caudal region of acute and chronic spinal cord injured rats treated by embryonic neural stem cells. *Physiol Res* **58**, 427-434
16. Maier, O., Bohm, J., Dahm, M., Bruck, S., Beyer, C., and Johann, S. (2013) Differentiated NSC-34 motoneuron-like cells as experimental model for cholinergic neurodegeneration. *Neurochem Int* **62**, 1029-1038
17. Lei, T., Du, S., Peng, Z., and Chen, L. (2022) Multifaceted regulation and functions of 53BP1 in NHEJ-mediated DSB repair (Review). *Int J Mol Med* **50**
18. Kleiner, R. E., Verma, P., Molloy, K. R., Chait, B. T., and Kapoor, T. M. (2015) Chemical proteomics reveals a gammaH2AX-53BP1 interaction in the DNA damage response. *Nat Chem Biol* **11**, 807-814
19. Chen, P. C., Ruan, J. S., and Wu, S. N. (2018) Evidence of Decreased Activity in Intermediate-Conductance Calcium-Activated Potassium Channels During Retinoic Acid-Induced Differentiation in Motor neuron-Like NSC-34 Cells. *Cell Physiol Biochem* **48**, 2374-2388
20. Madji Hounoum, B., Vourc'h, P., Felix, R., Corcia, P., Patin, F., Gueguinou, M., Potier-Cartereau, M., Vandier, C., Raoul, C., Andres, C. R., Mavel, S., and Blasco, H. (2016) NSC-34 Motor neuron-Like Cells Are Unsuitable as Experimental Model for Glutamate-Mediated Excitotoxicity. *Front Cell Neurosci* **10**, 118
21. Anjum, A. (2024) Mechanical scratch injury on differentiated motor neuron of NSC-34 cells as an in vitro model for evaluation of neuroregeneration potential of NeuroAiD II (MLC901). *Springer*
22. Nango, H., Kosuge, Y., Sato, M., Shibukawa, Y., Aono, Y., Saigusa, T., Ito, Y., and Ishige, K. (2020) Highly Efficient Conversion of Motor neuron-Like NSC-34 Cells into Functional Motor neurons by Prostaglandin E(2). *Cells* **9**
23. Nango, H., Kosuge, Y., Miyagishi, H., Sugawa, K., Ito, Y., and Ishige, K. (2017) Prostaglandin E2 facilitates neurite outgrowth in a motor neuron-like cell line, NSC-34. *J Pharmacol Sci* **135**, 64-71
24. Martinez, A. M., Mirkovic, J., Stanisz, Z. A., Patwari, F. S., and Yang, W. S. (2019) NSC-34 motor neuron-like cells are sensitized to ferroptosis upon differentiation. *FEBS Open Bio* **9**, 582-593

25. Kodirov, S. A. (2023) Whole-cell patch-clamp recording and parameters. *Biophys Rev* **15**, 257-288
26. Bucchia, M., Merwin, S. J., Re, D. B., and Kariya, S. (2018) Limitations and Challenges in Modeling Diseases Involving Spinal Motor neuron Degeneration in Vitro. *Front Cell Neurosci* **12**, 61
27. Kaur, G., and Dufour, J. M. (2012) Cell lines: Valuable tools or useless artifacts. *Spermatogenesis* **2**, 1-5
28. Richter, M., Piwocka, O., Musielak, M., Piotrowski, I., Suchorska, W. M., and Trzeciak, T. (2021) From Donor to the Lab: A Fascinating Journey of Primary Cell Lines. *Front Cell Dev Biol* **9**, 711381
29. Zakrzewski, W., Dobrzynski, M., Szymonowicz, M., and Rybak, Z. (2019) Stem cells: past, present, and future. *Stem Cell Res Ther* **10**, 68
30. da Silva, M. S. (2021) DNA Double-Strand Breaks: A Double-Edged Sword for Trypanosomatids. *Front Cell Dev Biol* **9**, 669041
31. Tuxworth, R. I., Taylor, M. J., Martin Anduaga, A., Hussien-Ali, A., Chatzimatthaiou, S., Longland, J., Thompson, A. M., Almutiri, S., Alifragis, P., Kyriacou, C. P., Kysela, B., and Ahmed, Z. (2019) Attenuating the DNA damage response to double-strand breaks restores function in models of CNS neurodegeneration. *Brain Commun* **1**, fcz005
32. Kinner, A., Wu, W., Staudt, C., and Iliakis, G. (2008) Gamma-H2AX in recognition and signaling of DNA double-strand breaks in the context of chromatin. *Nucleic Acids Res* **36**, 5678-5694
33. Popp, H. D., Brendel, S., Hofmann, W. K., and Fabarius, A. (2017) Immunofluorescence Microscopy of gammaH2AX and 53BP1 for Analyzing the Formation and Repair of DNA Double-strand Breaks. *J Vis Exp*
34. Rass, E., Willaume, S., and Bertrand, P. (2022) 53BP1: Keeping It under Control, Even at a Distance from DNA Damage. *Genes (Basel)* **13**
35. Falaschi, A., Chiaramonte, A., Testi, S., and Scarpato, R. (2023) Dual Immunofluorescence of gammaH2AX and 53BP1 in Human Peripheral Lymphocytes. *J Vis Exp*
36. Rassoolzadeh, H., Coucoravas, C., and Farnebo, M. (2015) The proximity ligation assay reveals that at DNA double-strand breaks WRAP53beta associates with gammaH2AX and controls interactions between RNF8 and MDC1. *Nucleus* **6**, 417-424
37. Ohno, M., Oka, S., and Nakabeppu, Y. (2009) Quantitative analysis of oxidized guanine, 8-oxoguanine, in mitochondrial DNA by immunofluorescence method. *Methods Mol Biol* **554**, 199-212
38. Shi, Z., Yuan, S., Shi, L., Li, J., Ning, G., Kong, X., and Feng, S. (2021) Programmed cell death in spinal cord injury pathogenesis and therapy. *Cell Prolif* **54**, e12992
39. Kyrylkova, K., Kyryachenko, S., Leid, M., and Kioussi, C. (2012) Detection of apoptosis by TUNEL assay. *Methods Mol Biol* **887**, 41-47
40. Rieger, A. M., Nelson, K. L., Konowalchuk, J. D., and Barreda, D. R. (2011) Modified annexin V/propidium iodide apoptosis assay for accurate assessment of cell death. *J Vis Exp*
41. Naso, M. F., Tomkowicz, B., Perry, W. L., 3rd, and Strohl, W. R. (2017) Adeno-Associated Virus (AAV) as a Vector for Gene Therapy. *BioDrugs* **31**, 317-334
42. Li, X., Le, Y., Zhang, Z., Nian, X., Liu, B., and Yang, X. (2023) Viral Vector-Based Gene Therapy. *Int J Mol Sci* **24**
43. Finneran, D. J., Njoku, I. P., Flores-Pazarin, D., Ranabothu, M. R., Nash, K. R., Morgan, D., and Gordon, M. N. (2021) Toward Development of Neuron Specific Transduction After Systemic Delivery of Viral Vectors. *Front Neurol* **12**, 685802

Acknowledgements – A.D. deeply appreciates daily supervisor E.S for the mentorship in the lab, the insightful discussions during the meetings and the assistance with data analysis, as well as promotor D.W. for his advice and support given throughout the internship.

Author contributions – A.D. would like to acknowledge his contributions to the cell culturing, quantitative PCR, and immunocytochemistry conducted in the laboratory. In the early stages, E.S. was instrumental in supporting the laboratory tasks. Throughout my internship, E.S. was a constant source of critical insights regarding experimental design and data interpretation whenever challenges arose. D.W. offered consistent direction on the experimental framework throughout the duration of my internship. The final manuscript was reviewed and approved by all contributors.

SUPPLEMENTARY

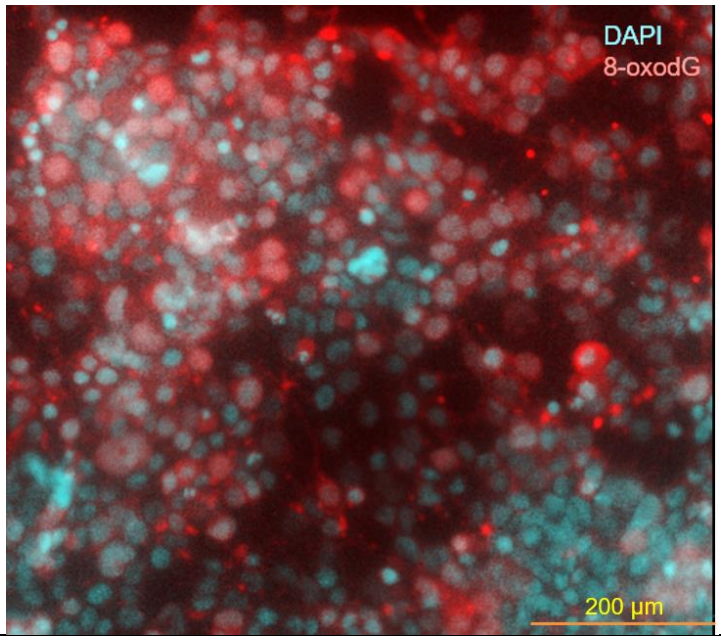

Figure 1: Failed 8-oxodG staining on NSC-34 motor neurons at 4hpi. After differentiating for 96 hours, the NSC-34 motor neurons were scratched and fixated at 4hpi. Unfortunately, the antibody rather stained the cell body than the nuclei and was therefore considered unspecific and excluded from further analysis.

Target	Sequence forward primer (5'- 3')	Sequence reverse primer (5' – 3')
YWHAZ	GCAACGATGTACTGTCTCTTT	GTCCACAATTCCTTTCTTGTCATC
GADPH	GGCCTTCCGTGTTCCTAC	TGTCATCATATCTGGCAGGTT
MAP2	TCTTTTGCTTGCTCGGGATT	TGCCACCTGTTTCTCTCCAC
MAPT	AAGGGGTATTGGGCAGAAGG	CTTTTCCTGTGGGAGCGAAG
GAP43	TAAGGAAAGTGCCCGACAGG	TGAGCAGGACAGGAGAGGAAA
CHAT	CCAACCAAGCCAAGCAATCT	AAGGATAGGGGAGCAGCAACAA
VACHT	GCGATGTGCTGCTTGATGA	TTGACCTAAATGGGGAGGGTA
ACHE	ACCTTCCCTGGCTTTTCCAC	GCATCCAACACTCCTGACCA
RBFOX3	ATCGTAGAGGGACGGAAAATTGA	GTTCCCAGGCTTCTTATTGGTC

Table 1: Overview of the various primers used to validate the differentiation of NSC34 cells to motor neurons by a qPCR analysis.

Table 2: Secondary antibodies used for ICC analysis

Secondary antibody	Supplier	Catalog number	Dilution
Goat anti-Rabbit-647	Invitrogen	A21245	1/800
Goat anti-Mouse-555	Invitrogen	A21245	1/800

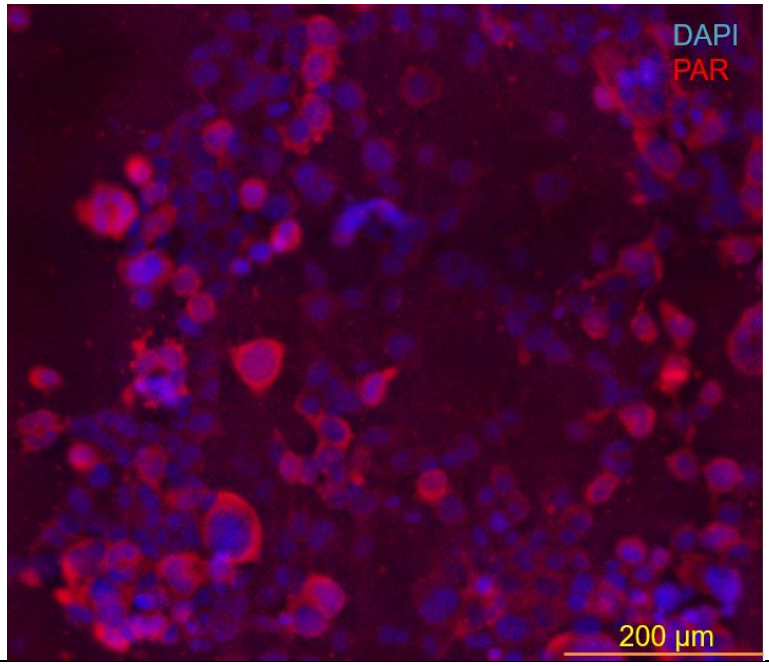

Figure 2: Unsuccessful PAR staining on NSC-34 motor neurons at 4hpi. Following a 96-hour differentiation period, the NSC-34 motor neurons were scratched and fixated at 4hpi. Unfortunately, the antibody predominantly targeted the cell body instead of the nuclei. This non-specific binding led to the decision to exclude the antibody from subsequent analyses.

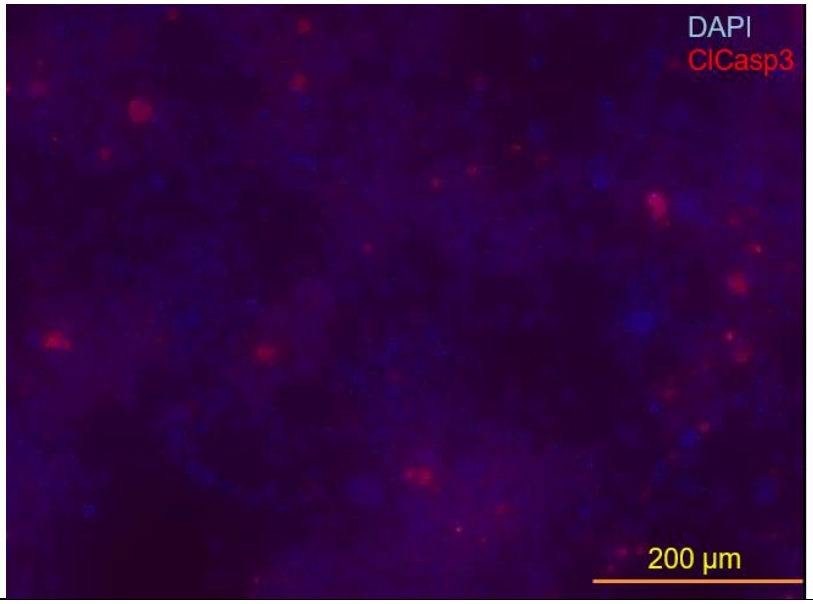

Figure 3: Successful clCasp3 staining on NSC-34 motor neurons at 4hpi. Following a 96-hour differentiation period, the NSC-34 motor neurons were scratched and fixated at 4hpi. The antibody targeted the nuclei, showing low levels of apoptosis.

```
open("C:/Users/Anouar/Downloads/53BP1_2hpi_A4_0016.nd2");
setOption("ScaleConversions", true);
run("8-bit");
run("Split Channels");
selectImage("C1-C:/Users/Anouar/Downloads/53BP1_2hpi_A4_0016.nd2");
run("Enhance Local Contrast (CLAHE)", "blocksize=127 histogram=256 maximum=3 mask=*None*
fast_(less_accurate)");
selectImage("C2-C:/Users/Anouar/Downloads/53BP1_2hpi_A4_0016.nd2");
run("Enhance Local Contrast (CLAHE)", "blocksize=127 histogram=256 maximum=3 mask=*None*
fast_(less_accurate)");
roiManager("Add");
roiManager("Select", 0);
selectImage("C1-C:/Users/Anouar/Downloads/53BP1_2hpi_A4_0016.nd2");
run("Gaussian Blur...", "sigma=5");
run("Subtract Background...", "rolling=50");
selectImage("C2-C:/Users/Anouar/Downloads/53BP1_2hpi_A4_0016.nd2");
run("Subtract Background...", "rolling=50");
selectImage("C1-C:/Users/Anouar/Downloads/53BP1_2hpi_A4_0016.nd2");
setAutoThreshold("Default dark no-reset");
//run("Threshold...");
setAutoThreshold("Otsu dark no-reset");
setThreshold(6, 255, "raw");
//setThreshold(6, 255);
setOption("BlackBackground", true);
run("Convert to Mask");
run("Watershed");
run("Analyze Particles...", "size=150-Infinity display exclude clear include summarize add");
selectImage("C2-C:/Users/Anouar/Downloads/53BP1_2hpi_A4_0016.nd2");
```

Table 3: Script for the analysis of the proportion of negative, foci and pan nuclear cells. Before utilizing this script, the file path should be changes manually. Additionally, it is necessary to manually establish the threshold value initially. Afterwards, the same threshold must be used for each specific marker.